Molecular Layer Deposition on Carbon Nanotubes

Joseph J. Brown,[†,*] Robert A. Hall,[‡] Paul E. Kladitis,[§] Steven M. George,[‡,†] and Victor M. Bright[†]

[†]Department of Mechanical Engineering, University of Colorado, 427 UCB, Boulder, Colorado 80309-0427, United States, [‡]Department of Chemistry and Biochemistry, University of Colorado, 215 UCB, Boulder, Colorado 80309-0215, United States, and [§]Department of Electrical Engineering, Air Force Institute of Technology, Wright Patterson Air Force Base, Ohio 45433, United States

ABSTRACT Molecular layer deposition (MLD) techniques were used to deposit conformal coatings on bulk quantities of carbon nanotubes (CNTs). Several metalcone MLD chemistries were employed, including alucone (trimethylaluminum/glycerol and trimethylaluminum/ethylene glycol), titanicone ($TiCl_4$/glycerol), and zincone (diethyl zinc/glycerol). The metalcone MLD films grew directly on the CNTs and MLD initiation did not require atomic layer deposition (ALD) of an adhesion layer. Transmission electron microscopy revealed that MLD formed three-dimensional conformal deposits throughout a CNT scaffold. Mechanical testing was also performed on sheets of CNT networks coated by MLD. Young's Modulus values improved from an initial value of 510 MPa for uncoated CNT sheet to values that ranged from 2.2 GPa, for 10 nm of glycerol alucone (AlGL), to 8.7 GPa for a composite 5 nm AlGL + 5 nm Al_2O_3 coating.

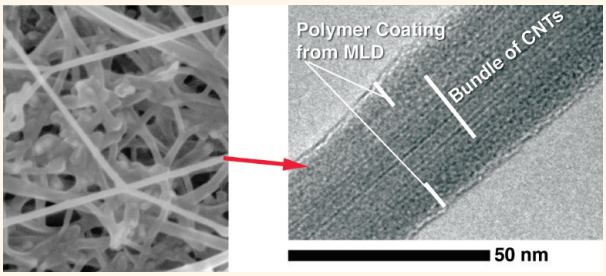

KEYWORDS: carbon nanotube · molecular layer deposition · ALD · mechanical testing · conformal · composite · scaffold

Translation of the interesting physical properties (high strength, high electrical conductivity, high current capacity, high thermal conductivity, low thermal expansion) of carbon nanotubes (CNTs) into useful macroscale applications has been a significant challenge since the inception of CNT research due to limitations on CNT availability and on the accessibility of technologies for measuring and utilizing the CNT properties in large-scale structures. Continual improvements in high volume carbon nanotube synthesis have resulted in current processes with sufficient yield to allow bulk testing and handling of carbon nanotubes. In bulk quantities, CNTs can provide a high surface area scaffolding material capable of supporting coatings that provide functionality for diverse new applications.[1,2] These include structural composites, stabilization for material handling, strain or gas sensing, tissue scaffolds, separations, drug delivery, environmental remediation, catalysis, chromatography, and battery and supercapacitor electrodes.[2,3]

CNTs are most commonly available as powders that may be dispersed in suspension and then collected into different ensemble forms. In other cases, CNTs are now available as forests on substrates, or as yarns or sheets. Spinning of CNT sheets with incorporated atomized titania and boron particles has been identified as one mechanism of formation of CNT bulk composites with optimized properties.[4] However, this mechanism is limited to only one structural modality, the formation of yarns or other linear structures.

A more versatile approach is to add coating technologies as processing steps after the initial bulk CNT shape-forming processes that generate sheets, filaments, or other modalities of CNT ensembles. Liquid coatings have been used to provide customizable surface treatments (such as polymer-derived ceramic formation) on some CNT materials,[1,5,6] but liquid-based processes can modify CNT forest shapes due to capillary forces.[7−9] Some larger polymer molecules such as PDMS and PVA will readily infiltrate microporous CNT network structures,[1] but these molecules may not reliably penetrate CNT bundles. Small molecules in liquid and gas phases may penetrate the tight, rope-like packing of single wall and double wall CNTs clumped into bundles in bulk ensembles.[10−13]

Gas phase deposition processes provide a complementary approach to conformal

* Address correspondence to joseph.j.brown@colorado.edu.

Received for review May 30, 2013 and accepted August 13, 2013.

Published online August 13, 2013
10.1021/nn402733g

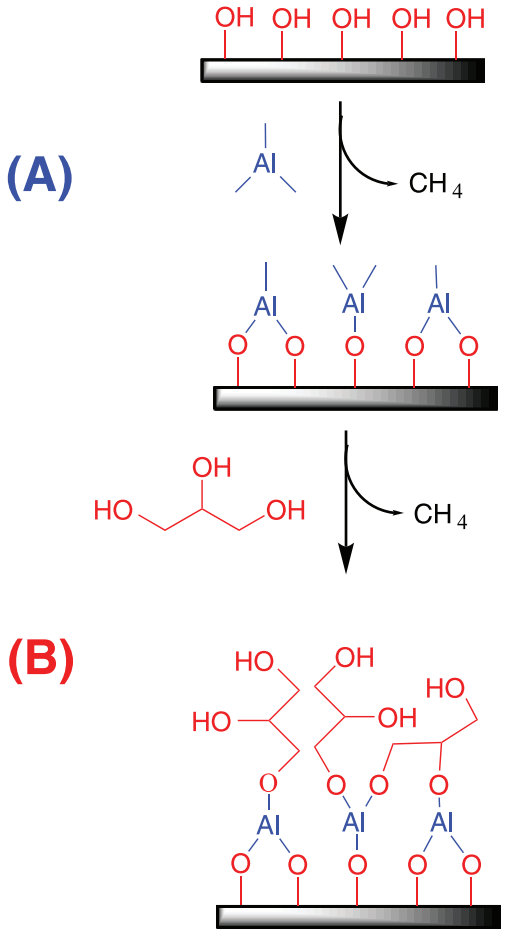

Figure 1. Scheme showing MLD process for generation of AlGL. Step A: A hydroxylated surface reacts with trimethylaluminum to generate a methylated aluminum surface and methane byproduct. Step B: The methylated aluminum surface reacts with glycerol to generate the polymer surface with hydroxyl termination. Steps A and B alternate, building up layers with thickness defined by the number of times the two steps are cycled. Nanotube substrates do not typically present hydroxylated surfaces. Adsorbed molecules are necessary for coating initiation on pristine nanotubes. For the MLD reactions presented here, adsorbed glycerol or ethylene glycol may play a role in coating initiation.

coating and bonding of CNTs. One such technology is atomic layer deposition (ALD), which deposits materials conformally based on the automated cycling of component gases.[14,15] The growth of individual layers is a self-limiting reaction, resulting in linear growth of material, with precise thickness dependent upon the number of ALD cycles exposed to the substrate. Molecular layer deposition (MLD, Figure 1) uses a similar approach to generate controlled-thickness conformal organic or hybrid organic–inorganic films, and can be deposited in combination with inorganic ALD layers.[16–18] The ALD and MLD processes are performed at relatively low temperatures, typically <200 °C.

MLD can be performed using a range of precursors to deposit polyamide, polyimide, and metal–organic polymer coatings such as alucones and zincones, which are hybrid polymers of metal ions (aluminum and zinc, respectively) bound to alcohols such as ethylene glycol or glycerol.[14,17] A variety of metals can be substituted into polymer layers grown with MLD. In fibrous scaffolds, the pore size may slow gaseous diffusion for ALD and MLD (or the related process of sequential vapor infiltration, SVI), but deposition has nonetheless been achieved on numerous fibrous materials, including polymers,[19–29] quartz fibers,[19] cellulose and cellulose acetate,[19–21,30–32] other biomaterials such as spider silk and collagen,[33–35] and carbon nanotubes.[36–44]

ALD has been demonstrated to add functionality to CNT scaffolds, generating nanoscale coaxial wires,[15,36] Pt catalytic systems,[37,43] lithium battery cathodes,[38,41] and stabilization of patterned CNT microstructures for chromatography and electrical vias.[39,44] MLD and ALD may be adapted for processing in an industrial environment, which is an important qualification for development of CNT composites and their applications. Large-scale processing with ALD has been incorporated in semiconductor electronics manufacturing processes[45,46] and ALD has been demonstrated on gram quantities of CNTs using a rotary reactor.[36]

Achieving a smooth, conformal coating has been one of the major challenges for ALD on CNTs. Without a nucleating layer, an alumina coating will typically nucleate in nodules, and smooth coatings are achieved after relatively thick (approximately 25 nm) deposits have been generated.[15] Thinner conformal coatings have been achieved when adsorbed molecules (for example, NO_2,[36,47] ozone[48]) are used to nucleate ALD coatings. However, films nucleated with NO_2 on CNTs can experience a "macaroni" effect allowing the film to slip off the CNT.[36]

Graphene presents similar challenges as CNTs with regards to ALD of continuous coatings. Graphene applications may benefit from the availability of additional mechanisms for generating conformal coatings. For conformal coatings on graphene, similar approaches are required as for CNTs. ALD initiation has been demonstrated on graphene with NO_2 and with an organic perylene-derivative monolayer.[49,50]

The work presented in this paper extends ALD technology to conformal deposition of metal alkoxide polymers on CNTs by use of molecular layer deposition (MLD). We found that MLD is capable of conformal deposition of coatings on CNTs without the use of initiator reagents to provide an adhesion layer. MLD films were deposited with trimethylaluminum (TMA) and glycerol (GL) or ethylene glycol (EG),[51,52] with diethyl zinc (DEZ) and GL,[52,53] or with titanium(IV) chloride ($TiCl_4$) and GL.[54]

Materials deposited by ALD and MLD have been subject to much mechanical characterization,[55–57] frequently through nanoindentation.[16,18,51–55,58–60] However, not many papers have explored ALD or MLD for mechanical applications in composite materials. With the use of nanoindentation, mechanical

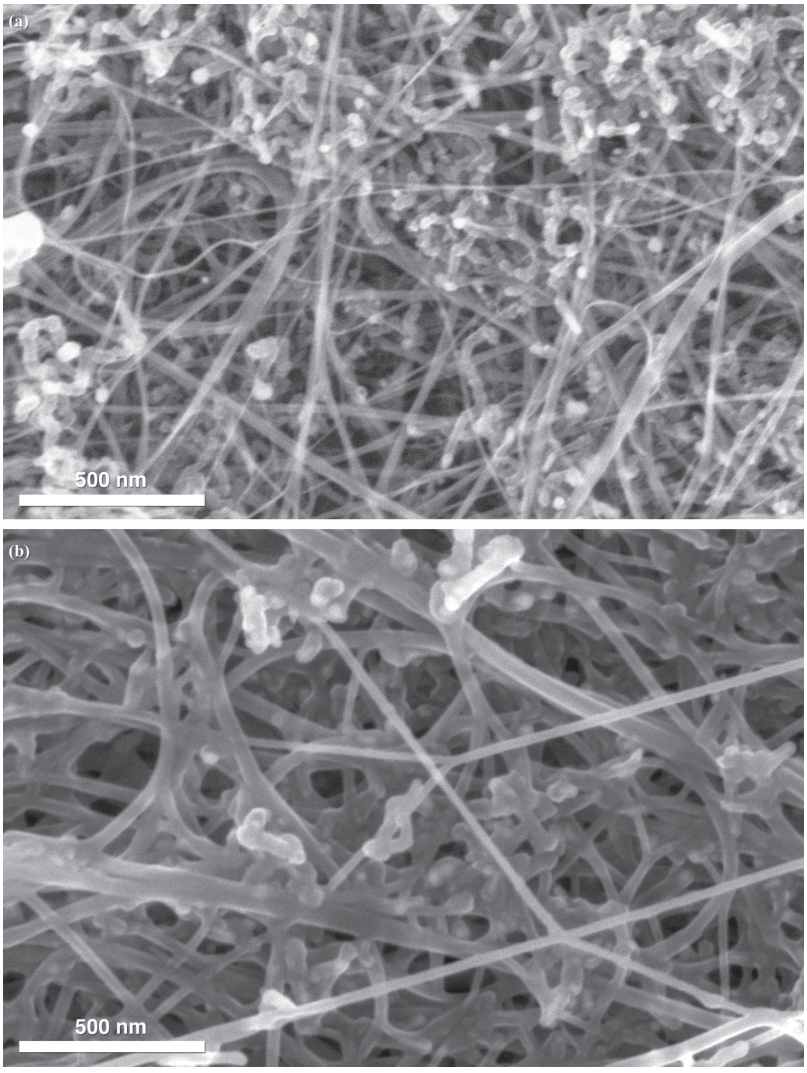

Figure 2. CNT sample (CNT1 sheet material) with (a) no coating and (b) 10 nm AlGL coating.

properties of nanoparticle thin films have been found to improve after ALD.[61−63] Furthermore, uniaxial tensile tests of bulk samples of polytetrafluoroethylene (PTFE) and two biopolymers, spider silk and collagen, showed that mechanical properties were improved by ALD and infiltration of ALD precursors.[29,33−35] Few other papers, if any, have explored the mechanical properties of ALD−fiber scaffold composites. We performed uniaxial tensile tests on both uncoated, as-provided CNT sheets and on CNT−MLD polymer composites, and we observed that MLD coatings significantly improved mechanical properties over uncoated bulk CNT scaffold structures.

RESULTS

Coatings of aluminum−glycerol (AlGL), aluminum−ethylene glycol (AlEG), titanium−glycerol (TiGL), and zinc−glycerol (ZnGL) were successfully deposited (Figure 2 and Supporting Information Figures S1 and S2) on carbon nanotube sheet specimens (CNT1 material). For deposition on CNT1, two types of reactor were used, designated as flow reactor and static reactor. Depositions of AlGL were also performed on CNT powder samples from three different sources (designated CNT2, CNT3, and CNT4). Deposition parameters and specific CNT sources are provided in the Methods section below. Molecular layer deposition produced conformal, smooth coatings on CNT1, CNT2, and CNT4, with very rare defects of balled or uncoated areas. Figure 2b shows typical coating results. Transmission electron microscope (TEM) imaging of CNT1 with AlGL coating confirms that the coating was capable of filling junctions between CNTs (Figure 3), both within bundles of CNTs and between bundles of CNTs. (Additional TEM images are available in Supporting Information Figure S3.)

Atomic layer deposition of Al_2O_3 was performed in order to check CNT materials' propensities for forming conformal coatings. Depositions of Al_2O_3 on CNT1, CNT2, and CNT4 formed rougher, more granular coatings than the AlGL, although smooth regions were occasionally present. In general, CNT3 did not accept

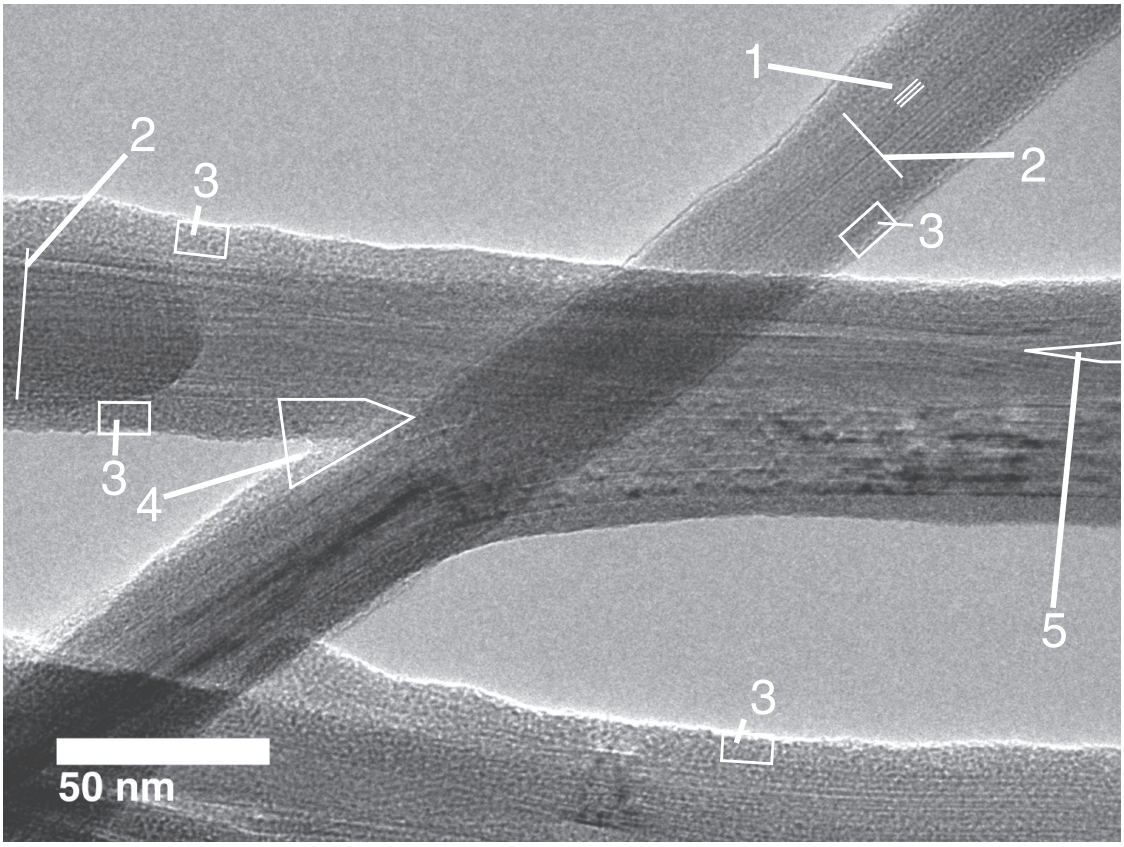

Figure 3. TEM image of CNT sheet (CNT1 material) coated with 10 nm AlGL. Annotations: (1) example of striations indicative of locations of CNT sidewalls visible in TEM image; (2) examples of bundles of CNTs; (3) some locations of AlGL coating on exterior of CNT bundles; (4) junction of CNT bundles where MLD AlGL forms a nanoscale fillet and spans the bundles; (5) location where MLD filled a loosely packed space between CNTs within a bundle.

any conformal coatings, with balled coating regions readily observed. ALD Al_2O_3 on CNT3 had worse coating quality than the AlGL; the alumina had more balling and less conformality. The AlGL layer was also used for successful nucleation of a smooth outer Al_2O_3 layer (Figures S4 and S5). Coatings of AlGL and ZnGL with 2, 4, 8, and 10 nm thicknesses were deposited in the flow reactor on CNT1 samples. For this range of coating thicknesses, coating morphology was not observed to vary significantly.

Focused ion beam (FIB) cross-sectioning of uncoated CNT sheet material was challenging, frequently appearing to destroy or densify the CNT sheet. However, cross sections of CNT sheet coated using MLD revealed coating throughout the thickness of the sheets, except in void regions in the sheets. Little difference was observed in the FIB cross sections that were obtained (Figure 4 and Figures S5–S7). Samples with thick (36.7 nm) AlGL coating were observed to have slightly smaller voids near their outer surfaces, and overall smoother surface features (Figure S1c) when compared with samples coated with 10 nm AlGL.

Energy-Dispersive Spectroscopy. Energy-dispersive X-ray spectroscopy (EDS) spectra obtained on the coated CNT1 samples confirmed the presence of metal ions in the different coatings (Table 1; Figures 5 and 6, and Figure S8). Quantitative analysis of EDS results (Table 1) found metal atom concentrations typically <10 atomic percent (atom %) for the MLD samples. In contrast, the Al_2O_3-coated sample had a much higher concentration of aluminum, about 19 atom %. As might be expected, the concentration of C increased from the Al_2O_3-coated sample to the AlEG-coated sample to the AlGL-coated sample. TiGL EDS showed the presence of trace quantities of Cl, 0.90 $\pm$ 0.03 atom %. Uncoated CNT1 sheet sample was 99 atom % C, 1 atom % Fe, with trace (0.1 atom %) S. Coated samples typically showed 1.0–2.3 atom % Fe catalyst, but to simplify comparisons, the Fe composition was excluded from the ratios presented in Table 1.

EDS spectra taken from points on fibers separated from bulk sheet samples typically show 5–10 atom % more carbon in composition than area scans of the bulk samples (Table 1). This indicates that the coating remained present on the separated fibers, but some of the coating may have been removed in the process of separation of the fiber from the larger mass. In contrast to the typical EDS point results, data collected on a sample of AlGL-coated CNTs in a TEM grid supported in a scanning transmission electron microscopy (STEM)

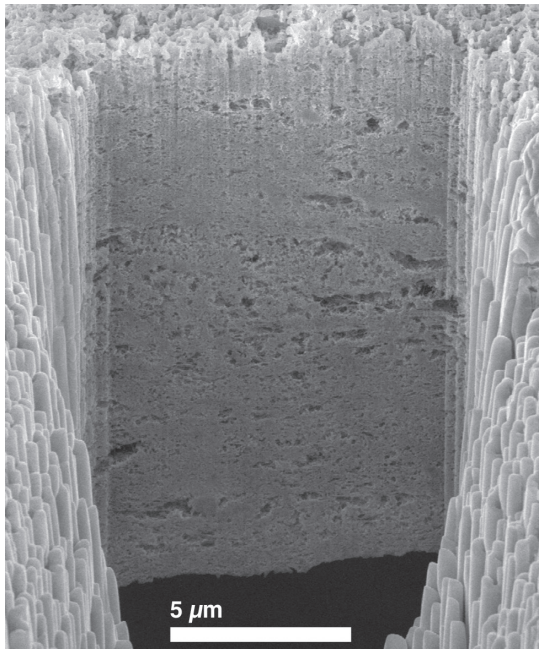

Figure 4. FIB cross section of 10 nm AlGL on a CNT1 sample, coated in static reactor, showing coating throughout the thickness of the CNT sheet sample. Stage tilt angle is 52° for this image.

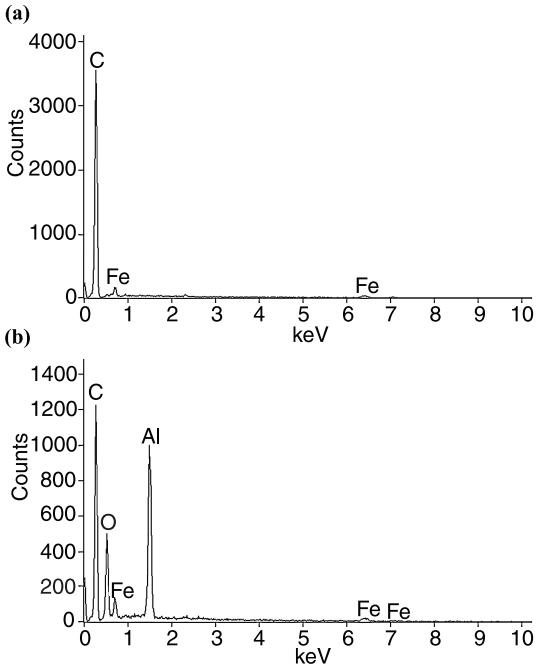

Figure 5. Comparison of EDS spectra of (a) uncoated CNT1 sheet and (b) CNT1 sheet coated with approximately 10 nm AlGL.

TABLE 1. EDS Compositional Analysis Results for Approximately 10 nm of Coatings on CNT1 Sheet[a]

coating	C [atom %]	O [atom %]	Me [atom %]	range [atom %]
Al_2O_3	48	34	19	±4
AlEG	72	19	9	±2
AlGL	83	11	6	±1
TiGl	87	8	4	±2
ZnGl	77	14	9	±1

[a] The metal ion Me percent refers to Al, Ti, or Zn, depending on the material.

stage and using 20 kV accelerating voltage showed lower carbon and aluminum content, and significantly more oxygen. In this instance, compositional analysis (Figure 6) found 72−77 atom % C, 21−26 atom % O, and 1.4−2.3 atom % Al. Given the presence of the significant Cu signal (Figure 6), these compositional values may differ from those in Table 2 in part because of a CuO layer on the surface of the grid used to support this sample.

Surface Treatment. To examine the effects on coating quality of possible surface contaminants from as-provided materials, the CNT materials were subjected to thermal treatments in flowing oxygen. One treatment was at 350 °C, intended to remove most adsorbed organic molecules. A second thermal treatment was performed at 560 °C, which was previously demonstrated to remove most of the amorphous carbon of CNT1 while leaving the CNTs intact.[64,65] In both cases, samples were supported in ceramic boats, and held at the temperatures for about 35 min before cooling back to room temperature. Samples of CNT1 were able to be processed in large enough quantities that washing the thermally treated samples with concentrated HCl(aq), followed by rinsing with H_2O, was possible. The transfer of Fe catalyst materials to ionic solution in HCl was readily observed by a color change in the HCl(aq) solution.

The results of these cleaning treatments were qualitatively observed by scanning electron microscope (SEM) imaging (FEI Nova 600i). As provided, CNT1 was a large network of CNTs with significant amorphous and particulate matter (Figure 2a). CNT2 was tangles of smooth CNTs, largely free of particulates. CNT3 was mostly particulate matter with fine, small CNTs interspersed. CNT4 was also largely tangles of CNTs, which appeared to have small quantities of amorphous material attached to the CNTs. The 350 °C processing had little effect on the CNT morphology, possibly giving some densification of samples. The 560 °C processing led to significant changes. CNT1 became a more delicate sheet material than prior to processing and exhibited little if any amorphous carbon, although some particulate matter remained. CNT2 and CNT3 became harder to find and possibly more packed, and the CNTs in sample CNT4 were eliminated, leaving only a particulate residue.

The HCl treatment removed particulates from the 560 °C treated CNT1 sample, resulting in a largely pure network of CNTs, but the HCl treatment was insufficient to remove particulates from CNT1 treated at 350 °C. Rapid coating experiments were performed by immobilizing these materials on TEM grids, and

then mounting multiple TEM grids in the flow reactor for simultaneous deposition. A coating of 10 nm AlGL was applied to the thermally treated materials. No major differences in AlGL coating morphology were observed between the treated and as-provided samples. On CNT1, 10 nm Al_2O_3 deposits appeared to be smoother for the HCl-treated 350 and 560 °C samples, and for the unwashed 560 °C sample, than for the as-provided material.

Mechanical Testing. The CNT1 samples were used for mechanical testing because they were provided as a sheet material that can be readily handled. The other samples were powder samples that would require further processing into buckypapers in order to be useful for macroscale mechanical testing. The CNT1 sheet samples had anisotropy that was evident in the mechanical data. They were fabricated by compressing a CNT aerogel produced as an output from a chemical vapor deposition furnace. Mechanical properties varied depending on whether the samples were tested in an axis parallel or perpendicular to the furnace output. Most of the results discussed here were from tests performed on samples loaded parallel to the sheet orientation.

Figure 7 summarizes the mechanical testing results for CNT1 sheet samples with different MLD coating treatments and tested under uniaxial tension parallel to the CNT sheet orientation. Numerical data for this figure are summarized in Supporting Information Table S1. Results for mechanical testing of samples perpendicular to the CNT1 sheet orientation may be found in Supporting Information Table S2.

The MLD coatings resulted in significant reduction in failure strain, modest improvement in ultimate tensile strength, and significant improvement in Young's Modulus by a factor that ranges from 4.3 (for AlGL) to 13.5 (for AlEG), in comparison to the untreated CNT1 material. The AlEG MLD coated CNT sample achieved the highest average Young's Modulus and ultimate tensile strength, 6.9 ± 2.2 GPa and 99 ± 43 MPa, respectively. The CNTs with AlGL coating achieved the greatest failure strain (3.92 ± 0.61%) of the MLD-treated samples. Testing of the composite AlGL−Al_2O_3-coated specimens revealed an even higher Young's Modulus, 8.7 ± 1.7 GPa, which is 17 times greater than that of the uncoated CNT sheet. Maximum Young's Modulus values for individual tests ranged up to 8.88 GPa for AlGL (flow reactor), 8.85 GPa for AlEG, and 11.3 GPa for AlGL−Al_2O_3. The highest ultimate tensile strength values obtained from individual tests on CNT−MLD polymer composites were 144 MPa for AlEG, 80.6 MPa for TiGL, and 98.2 MPa for AlGL−Al_2O_3.

DISCUSSION

Coating Quality. With the exception of the CNT3 specimens, molecular layer deposition provided a reliable and repeatable coating technology for CNT scaffolds, leading to observable changes in macroscale behavior.

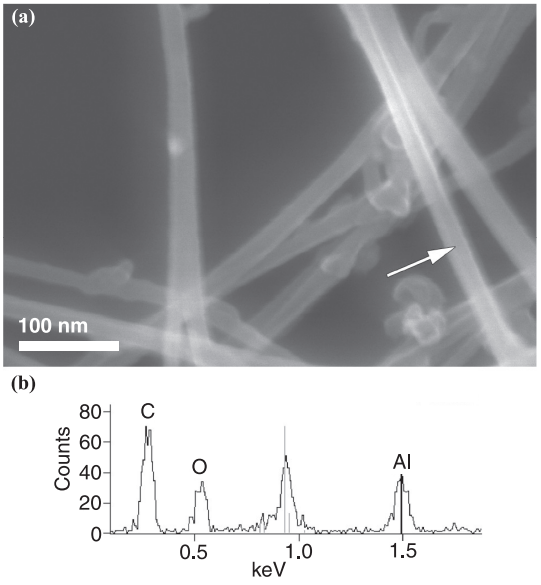

Figure 6. Point EDS of CNT1 sample with 10 nm AlGL coating, mounted in a TEM grid and an STEM holder. (a) SEM image of material sample. (b) EDS results for location indicated by arrow in (a). The unspecified peak at 0.9 keV is a Cu signal resulting from the TEM grid used to support this sample.

TABLE 2. Young's Modulus of Some Materials Generated by MLD, Measured by Thin Film Nanoindentation

material	Young's Modulus [GPa]	references
AlEG	36.8	55
AlGL	32.0	51, 52
TiGL	30.6	54
ZnGL	38.7	52, 53

The CNT3 specimens may be harder in general to coat due to their smaller diameter in comparison to the other materials. In CNTs, as diameter decreases, strain energy per atom increases proportional to the inverse square of the diameter.[66] At some small diameter, this strain energy may disrupt the uniform adhesion of molecules to the CNT substrates. Intermolecular forces in the adsorbed layer may then only be sufficient to draw the adsorbed molecules into clumps or droplets rather than maintaining a uniform coating.

The observation here of significant FIB damage to uncoated CNT sheets is similar to other observations of FIB on CNT networks.[67] In past work, the presence of a matrix surrounding the CNTs provided some stabilization of the FIB cross sections,[68,69] even if the CNT structure itself was damaged by the ion beam.[69,70] This appears to be the case as well for the CNT sheets with MLD coatings, and suggests that the MLD coatings may provide a means to stabilize scaffolding networks for FIB cutting.

The FIB cross sections (Figure 4 and Supporting Information Figures S5 and S6) show that the MLD precursors sufficiently penetrated the CNT scaffold layer

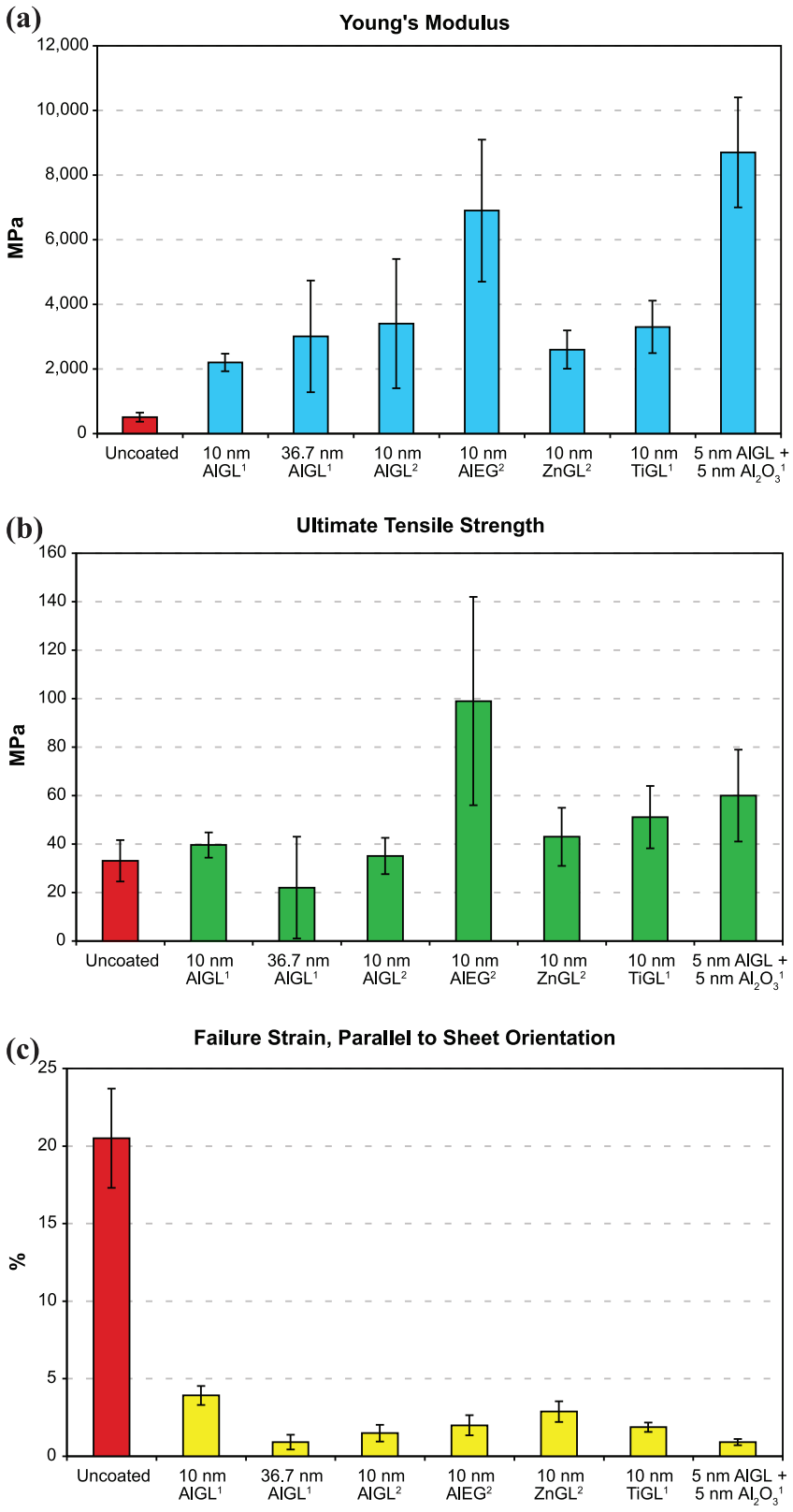

Figure 7. Uniaxial tensile test results for CNT1 sheet samples tested parallel to the sheet orientation. Values are reported in Table S1. Error bars indicate 95% confidence intervals. (1) Deposition in static reactor; (2) deposition in flow reactor. (a) Young's Modulus results; (b) ultimate tensile strength results; (c) failure strain results.

to deposit material throughout the thickness. However, the void spaces evident in the FIB cross sections indicate that one challenge with the as-provided CNT scaffolds is that they are not uniformly packed. This is not important

for the CNT powders, unless they are to be processed into a buckypaper for macroscopic handling. The CNT1 sheets may be readily handled in a laboratory setting, but further processing may ultimately be necessary to establish uniformity of thickness and packing density before undergoing MLD.

Improving the uniformity of the CNT scaffold may help reduce the variability in mechanical test results, and reduce stress concentrations that may be responsible for initiating failure in tested materials. Relatedly, the static reactor did not give greatly different mechanical results from the flow reactor, but the longer soak times of the static reactor did lead to more consistent results, with lower uncertainty. This may reflect the ability of the static reactor to better accommodate variability in the CNT sheet thickness.

We note that the cleaning processes did not have much of an effect on coating results. This observation indicates that the MLD coating process is independent of any potential adsorbed organic materials remaining from synthesis. One question not explored here was whether adsorbed gases from air lead to any effects on the MLD quality.

Other than achieving the most consistent results with samples coated with 10 nm AlGL in the static reactor, there was not a significant difference of stiffness among the AlGL-coated samples, whether with 10 nm or thicker coatings, or with static or flow reactor processing. Furthermore, the ZnGl and TiGl coatings result in composites with similar properties, regardless of whether the static or flow reactor was used for deposition. The difference between flow and static reactor processing was not readily evident in the mechanical data. In handling samples and picking at them with tweezers, samples processed in the flow reactor appeared to more frequently come apart into multiple layers, as if uncoated material lay at the center.

Mechanical Behavior. The tested coatings clearly have effects on the Young's Modulus and failure strain of the CNT1 sheet samples. For ultimate tensile strength, any effect is more ambiguous. The results for Young's Modulus are not simply explained by a rule of mixtures calculation based on known data (Table 2) about the MLD layers, however. If only the MLD layers carried load, then they would have about 10% of the total cross-sectional area in order to achieve the results reported in Table S1 (3 GPa results/30 GPa modulus = 10% of cross-sectional area bearing load, leaving 90% void space). From the FIB cross sections (Figure 4 and Supporting Information Figures S5 and S6), the polymer-coated regions clearly occupy much more than 10% of the overall area.

One explanation for this discrepancy between results and calculation could be that the polymer films have a different in-plane behavior than the out-of-plane behavior characterized by the nanoindenter. However, mechanical characterization of ALD alumina with other kinds of measurements has not observed anisotropy in the properties of these films.[49,56] Another explanation could just be that thickness and curvature-dependent variation in the coated film properties is not captured in the nanoindentation data reported in Table 2. Finally, the many voids present in the cross-section areas may allow for significant deformation (as the voids collapse during loading) that negates stiffening due to the coating and the CNT fibers.

The uncoated CNT1 sheet specimens are notable for their low Young's Modulus values and their extremely large strain to failure values. The failure strain behavior observed during tensile testing of these specimens is indicative of a polymer-like plastic deformation, wherein the CNT macromolecules pull past each other over a long distance before they ultimately fail. Assuming that the individual CNTs comprising this material have some high Young's Modulus on the order of 500−1000 GPa, the very low bulk Young's Modulus measured for the uncoated sheets again would seem to be a result of the insufficient packing of the sheets. Rather than testing a dense array of well-aligned CNTs, these tests are performed on a material of CNTs entangled together in a web-like structure. In a fiber reinforced composite, randomly oriented fibers in a sheet have three-eighths the modulus of aligned fibers.[71] Taking a low estimate for CNT modulus, 500 GPa, the randomly oriented fully packed sheet should have (3/8)(500) = 188 GPa modulus. With a 10% packing density, the sheet should still then have a modulus of 19 GPa. Even this is orders of magnitude larger than the measured value of 510 MPa. This discrepancy may be explained by several possibilities: (1) The assumed individual CNT stiffness may yet be overestimated, but this is unlikely because the bond strength of double-bonded carbon imparts significant rigidity to bonds within CNTs. (2) The bending curvature of CNTs and voids of the CNT sheet require further modification of the simple rigid fiber model. (3) The load transfer is insufficient between the CNTs; they are tangled and have short contact lengths, especially when considered in contrast to the lengths needed to fully transfer CNT load to CNT load.

With the MLD coatings added, the CNTs are reinforced against bending motion by the coating layers, and as observed in Figure 3, the coatings have filled in spaces between CNTs, possibly modifying the shear interactions between residual fibers. Both of these effects provide mechanisms that may offer some explanation in the improvement of mechanical properties observed in the composite sheets, in addition to the possibility of load-bearing by the alkoxide polymer matrices themselves. All of these effects warrant further investigation. Because the deposit of a thick AlGL coating did not lead to results much different from a 10 nm coating, an interesting route for later investigation may be to find the minimum coating thickness required to significantly modify the properties of the composited sheet.

From a practical standpoint, we note that handling the coated CNT sheets is much easier than handling the uncoated material. The uncoated CNT sheet material tends to stick to itself fairly readily. In contrast, the coated materials are more rigid, as is evident in the reported data, and their macroscopic behavior is similar to that of rigid polymer films. The MLD-coated CNT films are easier to handle, tape, and cut than the uncoated films, suggesting an application of MLD as a means to stabilize material networks of CNTs for improved handling.

CONCLUSIONS

Conformal deposition of metal alkoxide polymers by molecular layer deposition has been repeatedly demonstrated on multiple CNT specimens. These coatings typically generate conformal films and TEM data reveals that they are capable of filling spaces and junctions between CNTs and in bundles of CNTs. Coatings of AlEG, AlGL, ZnGL, and TiGL were successfully deposited on CNT scaffolds, and EDS confirmed presence of metal ions in the coatings. A layer of 5 nm AlGL on CNT scaffold was also used to achieve nucleation of a conformal coating of an additional 5 nm of Al_2O_3 that was deposited by ALD.

Macroscopic sheet samples were made easier to handle by MLD, and were subjected to tensile testing under a controlled strain rate in a DMA. The Young's Modulus values of the macroscopic sheet samples improved from a starting value of 510 $\pm$ 140 MPa to results that ranged from 2.20 $\pm$ 0.27 GPa for 10 nm AlGL to the best result, 8.7 $\pm$ 1.7 GPa, for the composite 5 nm AlGL + 5 nm Al_2O_3 coating. In addition to demonstration of improvement of material handling and a new route to fabrication of a macroscale CNT–polymer composite with mechanical properties improved relative to uncoated CNT networks, this work suggests great possibilities for additional routes of investigation.

MLD may be applicable to developing many additional coatings for CNT scaffolds, including thiol- and quinone-based chemistries. The observation of conformal coatings from MLD on CNTs suggests that the interplay of surface energy, surface curvature, adsorption, and vapor pressure should be explored in order to develop a quantitative theory for ALD/MLD nucleation, perhaps drawing upon concepts such as the Tolman length, which is relevant to nanoscale systems. Further work can be done developing a detailed mechanical model that describes networks of CNTs in polymer composites, whether formed by MLD or otherwise. Further development of CNT packing and macromaterial uniformity should be investigated for improvements in mechanical properties of the macroscale material, although this may make MLD more difficult by limiting the channel size available for gaseous diffusion. Exploration of controlled environments preventing air exposure to CNTs before deposition may also be an interesting route of investigation. Finally, coated networks based on CNT scaffolding should be explored for applications requiring high surface area functionality, such as sensing, separations, chemical processing, and electrodes, and MLD should be explored for coating deposition on additional carbon allotropes such as graphene.

METHODS

Materials and Chemical Systems. The chemicals used for the fabrication of the AlGL, ZnGL, and TiGL films were trimethylaluminum ($Al(CH_3)_3$; 97%, Sigma Aldrich), diethyl zinc ($Zn(CH_2CH_3)_2$; Aldrich) titanium(IV) chloride ($TiCl_4$; 99%, Sigma Aldrich), and glycerol ($(HOCH_2)_2CHOH$; 99%, Sigma Aldrich). Deposition of AlEG used trimethylaluminum and ethylene glycol ($HO(CH_2)_2OH$; Reagent Plus >99%, Sigma Aldrich). The carrier gas used was ultra high purity N_2 (Airgas). (*Caution*: Trimethylaluminum and diethyl zinc are pyrophoric, and titanium(IV) chloride is corrosive. Safe handling requires proper exhaust of ALD/MLD deposition reactor outflow, leak checking before reactor operation, and use of purge gases to prevent gas phase mixing of reagents. ALD and MLD hazards are mitigated using a nitrogen flow in a reaction chamber that is isolated from the atmospheric gases during pumping. Gases are dosed using a leak-free piping system that ensures gas control and isolation.) Deposition experiments were performed on CNTs from the following four sources:

Sample CNT1: Standard CNT sheet material, lot number Ah-3CV (obtained in 2011), from NanoComp Technologies (Merrimack, NH).

Sample CNT2: Multiwalled CNTs, item #43839, Alfa Aesar (Ward Hill, MA).

Sample CNT3: Single-walled CNTs, item #44508, Alfa Aesar.

Sample CNT4: Multiwalled CNTs, 7000 series, Nanocyl (Sambreville, Belgium).

Depositions were performed on as-provided materials, unless additional processing is noted. The CNT4 material was previously used for experiments reported in ref 36. CNT materials were handled in air. CNT1 sheets were fixed in place using polyimide tape at the edges of the sheets. Other CNT samples were supported on Cu TEM grids that were mechanically clamped in the reactors.

CNTs were placed in either a viscous flow reactor or a static reactor; these reactors were described in earlier work.[36,72] For the viscous flow reactor, the TMA was maintained at 25 °C and a temperature gradient was maintained up to the reactor temperature of 150 °C. The GL was heated to 120 °C and a temperature gradient was maintained up to the reactor temperature of 150 °C. The GL necessitated heating to this temperature because of its inherent low vapor pressure. Dosing for one cycle takes the form of {Dose A/Purge N_2/Dose B/Purge N_2}. For AlGL (Figure 1), the deposition parameters used for the viscous flow reactor were {2 s TMA/120 s/0.5 s GL/120 s}. The growth rate was approximately 2.4 Å/cycle for AlGL deposition. The conditions were changed for ZnGL deposition and were {1 s DEZ/30 s/1 s GL/30 s}. The growth rate at 150 °C for ZnGL was 1.3 Å/cycle at 150 °C. The conditions for TiGL were {1 s $TiCl_4$/30 s/1 s GL/30 s} with a growth rate of 2.2 Å/cycle at 150 °C. For Al_2O_3 deposition, the parameters were {1 s TMA/30 s/1 s H_2O/30 s} with a growth rate of 1.1 Å/cycle at 130 °C. The alucone AlEG MLD films were deposited using {0.5 s TMA/120 s/1.5 s EG dose/120 s} as the reaction parameters, with growth rates of 2.5 Å/cycle at 100–120 °C. The AlEG dose times produced TMA pressure transients of approximately 130 mTorr and EG pressure transients of approximately 70 mTorr above the baseline pressure.

The conditions were changed slightly to accommodate the static deposition reactor. The reactor was maintained at 150 °C but instead of having continuous flow, the reactant doses were held for a predetermined time and then purged from the reactor. This allows for the reactants to penetrate into very high aspect structures such as CNT sheets or papers. The dosing process takes a different form and follows: A = {Dose A/Static Time/Purge Time} and B = {Dose B/Static Time/Purge Time}. Each of the half cycles is followed by an additional purge cycle that is the same for both half cycles: 20 s N_2 dose/5 s N_2 static hold/45 s N_2 pump purge/20 s hold. This was repeated 5 times per half cycle. For the AlGL reaction, the dosing parameters were {2 s TMA/60 s/60 s}{2 s GL/240 s/240 s}. These conditions gave a much larger growth rate of about 6 Å/cycle. For the ZnGL and TiGL reactions, the dosing parameters were the same.

Microscopic Analysis. Focused ion beam (FIB) cross-sectioning was performed using an FEI Nova 600i dual beam focused ion beam scanning electron microscope (FIB-SEM). Quantitative energy dispersive X-ray spectroscopy (EDS) was performed on coated CNT sheets using a JEOL JSM-7401F field emission scanning electron microscope (FESEM) running 10 kV accelerating voltage, with data collection and analysis by a Thermo Scientific NORAN System SIX EDS system. Results were determined by averaging EDS results from area scans in two locations on each surface of coated sheet. EDS data were rounded to the nearest percent because typical results showed at least a percent difference between the carbon composition at the different locations of each sample. Composition ranges are reported as ±atomic percent (atom %) around the reported average. SEM images were acquired primarily with the FEI Nova 600i; the JEOL JSM-7401F provided additional SEM data during the EDS analysis. TEM images were acquired using a JEOL 2000 FX with LaB_6 cathode.

Mechanical Experiments. Mechanical testing was performed by cutting coated and uncoated samples of CNT1 sheet material into rectangular test specimens approximately 5 mm × 20 mm in size. Specimen width was measured directly from calipers, and specimen thickness was defined by the average of 10 thickness caliper measurements. Because of the large number of specimens tested, specimens cut from adjacent regions of CNT sheet material were assumed to have the same thickness; measured thickness of one specimen was also used for the thickness of neighboring specimens.

Mechanical testing was performed using a dynamic mechanical analyzer (DMA; TA Instruments Q800). All tests were performed using a constant strain rate of 6% min^{-1} (10^{-3} s^{-1}). Gauge lengths were measured by the DMA for each sample before testing. Each tensile test in the DMA produced a tensile plot, and from each tensile plot, the maximum slope defined the Young's Modulus measured for that test, and the ultimate tensile strength and failure strain were also determined. The data reported were found by averaging the results obtained for a number of samples, *N*. Uncertainty was calculated from the standard deviation of the mean, multiplied by a coverage factor defined by the two-sided Student *t* variable for 95% probability and $N - 1$ degrees of freedom.

Conflict of Interest: The authors declare the following competing financial interest: J.J. Brown helped found NanoComp Technologies in 2004, and worked there as Senior Engineer in 2004-2006; he continues to be a minor shareholder of this company.

Supporting Information Available: (1) Data tables for mechanical test results parallel and perpendicular to the CNT sheet orientation; (2) additional SEM and TEM images of coated CNT materials; (3) additional EDS spectra of MLD coatings on CNTs, and comparison to Al_2O_3 ALD coating on CNTs. This material is available free of charge *via* the Internet at http://pubs.acs.org.

Acknowledgment. The authors acknowledge the following individuals and organizations for assistance and helpful discussions regarding this work: D. Lashmore, University of New Hampshire; NanoComp Technologies, Inc.; R. Geiss, NIST—Boulder, for TEM imaging and EDS for Figure 6; and B. Landi, Rochester Institute of Technology. Funding support for J.J.B. was provided by the U.S. Government Intelligence Community Postdoctoral Research Fellowship Program. Funding support for R.A.H. was provided by DARPA.

REFERENCES AND NOTES

1. Gui, X.; Cao, A.; Wei, J.; Li, H.; Jia, Y.; Li, Z.; Fan, L.; Wang, K.; Zhu, H.; Wu, D. Soft, Highly Conductive Nanotube Sponges and Composites with Controlled Compressibility. *ACS Nano* **2010**, *4*, 2320–2326.
2. Nardecchia, S.; Carriazo, D.; Ferrer, M. L.; Gutiérrez, M. C.; del Monte, F. Three Dimensional Macroporous Architectures and Aerogels Built of Carbon Nanotubes and/or Graphene: Synthesis and Applications. *Chem. Soc. Rev.* **2013**, *42*, 794–830.
3. Roy, S.; Jain, V.; Bajpai, R.; Ghosh, P.; Pente, A. S.; Singh, B. P.; Misra, D. S. Formation of Carbon Nanotube Bucky Paper and Feasibility Study for Filtration at the Nano and Molecular Scale. *J. Phys. Chem. C.* **2012**, *116*, 19025–19031.
4. Lima, M. D.; Fang, S.; Lepró, X.; Lewis, C.; Ovalle-Robles, R.; Carretero-González, J.; Castillo-Martínez, E.; Kozlov, M. E.; Oh, J.; Rawat, N.; *et al.* Biscrolling Nanotube Sheets and Functional Guests into Yarns. *Science* **2011**, *331*, 51–55.
5. Shah, S. R.; Raj, R. Nanodevices That Explore the Synergies Between PDCs and Carbon Nanotubes. *J. Eur. Ceram. Soc.* **2005**, *25*, 243–249.
6. Singh, G.; Priya, S.; Hossu, M. R.; Shah, S. R.; Grover, S.; Koymen, A. R.; Mahajan, R. L. Synthesis, Electrical and Magnetic Characterization of Core—Shell Silicon Carbo-Nitride Coated Carbon Nanotubes. *Mater. Lett.* **2009**, *63*, 2435–2438.
7. De Volder, M.; Tawfick, S. H.; Park, S. J.; Copic, D.; Zhao, Z.; Lu, W.; Hart, A. J. Diverse 3D Microarchitectures Made by Capillary Forming of Carbon Nanotubes. *Adv. Mater.* **2010**, *22*, 4384–4389.
8. De Volder, M. F. L.; Tawfick, S.; Park, S. J.; Hart, A. J. Corrugated Carbon Nanotube Microstructures with Geometrically Tunable Compliance. *ACS Nano* **2011**, *5*, 7310–7317.
9. García, E. J.; Hart, A. J.; Wardle, B. L.; Slocum, A. H. Fabrication of Composite Microstructures by Capillarity-Driven Wetting of Aligned Carbon Nanotubes with Polymers. *Nanotechnology* **2007**, *18*, 165602.
10. Esteves, I. A. A. C.; Cruz, F. J. A. L.; Müller, E. A.; Agnihotri, S.; Mota, J. P. B. Determination of the Surface Area and Porosity of Carbon Nanotube Bundles from a Langmuirian Analysis of Sub- and Supercritical Adsorption Data. *Carbon* **2009**, *47*, 948–956.
11. Böttcher, A.; Hennrich, F.; Rösner, H.; Malik, S.; Kappes, M. M.; Lichtenberg, S.; Schoch, G.; Deutschmann, O. Growth of Novel Carbon Phases by Methane Infiltration of Free-Standing Single-Walled Carbon Nanotube Films. *Carbon* **2007**, *45*, 1085–1096.
12. Hedderman, T. G.; Mostaert, A. S.; Shanahan, A. E.; Byrne, H. J. The Dispersion of SWCNT Bundles on Interaction with *p*-Terphenyl. *New Carbon Mater.* **2009**, *24*, 73–82.
13. Fang, C.; Zhao, J.; Jia, J.; Zhang, Z.; Zhang, X.; Li, Q. Enhanced Carbon Nanotube Fibers by Polyimide. *Appl. Phys. Lett.* **2010**, *97*, 181906.
14. George, S. M. Atomic Layer Deposition: An Overview. *Chem. Rev.* **2010**, *110*, 111–131.
15. Hermann, C. F.; Fabreguette, F. H.; Finch, D. S.; Geiss, R.; George, S. M. Multilayer and Functional Coatings on Carbon Nanotubes Using Atomic Layer Deposition. *Appl. Phys. Lett.* **2005**, *87*, 125110.
16. George, S. M.; Lee, B. H.; Yoon, B.; Abdulagatov, A. I.; Hall, R. A. Metalcones: Hybrid Organic-Inorganic Films Fabricated Using Atomic and Molecular Layer Deposition Techniques. *J. Nanosci. Nanotechnol.* **2011**, *11*, 7948–7955.
17. Liang, X.; King, D. M.; Li, P.; George, S. M.; Weimer, A. W. Nanocoating Hybrid Polymer Films on Large Quantities of Cohesive Nanoparticles by Molecular Layer Deposition. *AIChE J.* **2009**, *55*, 1030–1039.

18. Lee, B. H.; Yoon, B.; Anderson, V. R.; George, S. M. Alucone Alloys with Tunable Properties Using Alucone Molecular Layer Deposition and Al_2O_3 Atomic Layer Deposition. *J. Phys. Chem. C* **2012**, *116*, 3250–3257.
19. Jur, J. S.; Sweet, W. J., III; Oldham, C. J.; Parsons, G. N. Atomic Layer Deposition of Conductive Coatings on Cotton, Paper, and Synthetic Fibers: Conductivity Analysis and Functional Chemical Sensing Using "All-Fiber" Capacitors. *Adv. Funct. Mater.* **2011**, *21*, 1993–2002.
20. Roy, A. K.; Deduytsche, D.; Detavernier, C. Wetting Transitions of Polymers *via* Thermal and Plasma Enhanced Atomic Layer Depositions. *J. Vac. Sci. Technol., A* **2013**, *31*, 01A147.
21. Oldham, C. J.; Gong, B.; Spagnola, J. C.; Jur, J. S.; Senecal, K. J.; Godfrey, T. A.; Parsons, G. N. Encapsulation and Chemical Resistance of Electrospun Nylon Nanofibers Coated Using Integrated Atomic and Molecular Layer Deposition. *J. Electrochem. Soc.* **2011**, *158*, D549–D556.
22. Musschoot, J.; Dendooven, J.; Deduytsche, D.; Haemers, J.; Buyle, G.; Detavernier, C. Conformality of Thermal and Plasma Enhanced Atomic Layer Deposition on a Non-Woven Fibrous Substrate. *Surf. Coat. Technol.* **2012**, *206*, 4511–4517.
23. Donmez, I.; Kayaci, F.; Ozgit-Akgun, C.; Uyar, T.; Biyikli, N. Fabrication of Hafnia Hollow Nanofibers by Atomic Layer Deposition Using Electrospun Nanofiber Templates. *J. Alloys Compd.* **2013**, *559*, 146–151.
24. Gong, B.; Peng, Q.; Parsons, G. N. Conformal Organic-Inorganic Hybrid Network Polymer Thin Films by Molecular Layer Deposition using Trimethylaluminum and Glycidol. *J. Phys. Chem. B* **2011**, *115*, 5930–5938.
25. Kayaci, F.; Ozgit-Akgun, C.; Donmez, I.; Biyikli, N.; Uyar, T. Polymer–Inorganic Core–Shell Nanofibers by Electrospinning and Atomic Layer Deposition: Flexible Nylon–ZnO Core–Shell Nanofiber Mats and Their Photocatalytic Activity. *ACS Appl. Mater. Interfaces* **2012**, *4*, 6185–6194.
26. Gong, B.; Peng, Q.; Jur, J. S.; Devine, C. K.; Lee, K.; Parsons, G. N. Sequential Vapor Infiltration of Metal Oxides into Sacrificial Polyester Fibers: Shape Replication and Controlled Porosity of Microporous/Mesoporous Oxide Monoliths. *Chem. Mater.* **2011**, *23*, 3476–3485.
27. Liang, X.; George, S. M.; Weimer, A. W.; Li, N.-H.; Blackson, J. H.; Harris, J. D.; Li, P. Synthesis of a Novel Porous Polymer/Ceramic Composite Material by Low-Temperature Atomic Layer Deposition. *Chem. Mater.* **2007**, *19*, 5388–5394.
28. Sweet, W. J., III; Jur, J. S.; Parsons, G. N. Bi-Layer Al_2O_3/ZnO Atomic Layer Deposition for Controllable Conductive Coatings on Polypropylene Nonwoven Fiber Mats. *J. Appl. Phys.* **2013**, *113*, 194303.
29. Lee, S.-M.; Ischenko, V.; Pippel, E.; Masic, A.; Moutanabbir, O.; Fratzl, P.; Knez, M. An Alternative Route Towards Metal–Polymer Hybrid Materials Prepared by Vapor-Phase Processing. *Adv. Funct. Mater.* **2011**, *21*, 3047–3055.
30. Hanson, C. A.; Oldham, C. J.; Parsons, G. N. Paper Deacidification and UV Protection Using ZnO Atomic Layer Deposition. *J. Vac. Sci. Technol., A* **2012**, *30*, 01A117.
31. Hyde, G. K.; McCullen, S. D.; Jeon, S.; Stewart, S. M.; Jeon, H.; Loboa, E. G.; Parsons, G. N. Atomic Layer Deposition and Biocompatibility of Titanium Nitride Nano-Coatings on Cellulose Fiber Substrates. *Biomed. Mater.* **2009**, *4*, 025001.
32. Hyde, G. K.; Stewart, S. M.; Scarel, G.; Parsons, G. N.; Shih, C.-C.; Shih, C.-M.; Lin, S.-J.; Su, Y.-Y.; Monteiro-Riviere, N. A.; Narayan, R. J. Atomic Layer Deposition of Titanium Dioxide on Cellulose Acetate for Enhanced Hemostasis. *Biotechnol. J.* **2011**, *6*, 213–223.
33. Lee, S.-M.; Pippel, E.; Gösele, U.; Dresbach, C.; Qin, Y.; Chandran, C. V.; Bräuniger, T.; Hause, G.; Knez, M. Greatly Increased Toughness of Infiltrated Spider Silk. *Science* **2009**, *324*, 488–492.
34. Lee, S.-M.; Pippel, E.; Moutanabbir, O.; Gunkel, I.; Thurn-Albrecht, T.; Knez, M. Improved Mechanical Stability of Dried Collagen Membrane after Metal Infiltration. *ACS Appl. Mater. Interfaces* **2010**, *2*, 2436–2441.
35. Lee, S.-M.; Pippel, E.; Knez, M. Metal Infiltration into Biomaterials by ALD and CVD: A Comparative Study. *ChemPhysChem* **2011**, *12*, 791–798.
36. Cavanagh, A. S.; Wilson, C. A.; Weimer, A. W.; George, S. M. Atomic Layer Deposition on Gram Quantities of Multi-Walled Carbon Nanotubes. *Nanotechnology* **2009**, *20*, 255602.
37. Dameron, A. A.; Pylypenko, S.; Bult, J. B.; Neyerlin, K. C.; Engtrakul, C.; Bochert, C.; Leong, G. J.; Frisco, S. L.; Simpson, L.; Dinh, H. N.; *et al.* Aligned Carbon Nanotube Array Functionalization for Enhanced Atomic Layer Deposition of Platinum Electrocatalysts. *Appl. Surf. Sci.* **2012**, *258*, 5212–5221.
38. Chen, X.; Zhu, H.; Chen, Y.-C.; Shang, Y.; Cao, A.; Hu, L.; Rubloff, G. W. MWCNT/V_2O_5 Core/Shell Sponge for High Areal Capacity and Power Density Li-Ion Cathodes. *ACS Nano* **2012**, *6*, 7948–7955.
39. Fayolle, M.; Poncharra, J.; Dijon, J.; Fournier, A.; Okuno, H.; Quesnel, E.; Muffato, V.; Jayet, C.; Lugand, J. F.; Gautier, P.; *et al.* Innovative Scheme for Selective Carbon Nanotubes Integration in Via Structures. *Microelectron. Eng.* **2011**, *88*, 833–836.
40. Devine, C. K.; Oldham, C. J.; Jur, J. S.; Gong, B.; Parsons, G. N. Fiber Containment for Improved Laboratory Handling and Uniform Nanocoating of Milligram Quantities of Carbon Nanotubes by Atomic Layer Deposition. *Langmuir* **2011**, *27*, 14497–14507.
41. Meng, X.; Liu, J.; Banis, M. N.; Yang, J.; Li, R.; Sun, X. Atomic Layer Deposited $Li_4Ti_5O_{12}$ on Nitrogen-Doped Carbon Nanotubes. *RSC Adv.* **2013**, *3*, 7285–7288.
42. Meng, X.; Banis, M. N.; Geng, D.; Li, X.; Zhang, Y.; Li, R.; Abou-Rachid, H.; Sun, X. Controllable Atomic Layer Deposition of One-Dimensional Nanotubular TiO_2. *Appl. Surf. Sci.* **2013**, *266*, 132–140.
43. Liu, C.; Wang, C.-C.; Kei, C.-C.; Hsueh, Y.-C.; Perng, T.-P. Atomic Layer Deposition of Platinum Nanoparticles on Carbon Nanotubes for Application in Proton-Exchange Membrane Fuel Cells. *Small* **2009**, *5*, 1535–1538.
44. Jensen, D. S.; Kanyal, S. S.; Gupta, V.; Vail, M. A.; Dadson, A. E.; Engelhard, M.; Vanfleet, R.; Davis, R. C.; Linford, M. R. Stable, Microfabricated Thin Layer Chromatography Plates Without Volume Distortion on Patterned, Carbon and Al_2O_3-Primed Carbon Nanotube Forests. *J. Chromatogr., A* **2012**, *1257*, 195–203.
45. Poodt, P.; Lankhorst, A.; Roozeboom, F.; Spee, K.; Maas, D.; Vermeer, A. High-Speed Spatial Atomic-Layer Deposition of Aluminum Oxide Layers for Solar Cell Passivation. *Adv. Mater.* **2010**, *22*, 3564–3567.
46. Verghese, M.; Maes, J. W.; Kobayashi, N. Atomic Layer Deposition Goes Mainstream in 22 nm Logic Technologies. *Solid State Technol.* **2010**, *53*, 18–21.
47. Farmer, D. B.; Gordon, R. G. Atomic Layer Deposition on Suspended Single-Walled Carbon Nanotubes *via* Gas Phase Noncovalent Functionalization. *Nano Lett.* **2006**, *6*, 699–703.
48. Jandhyala, S.; Mordi, G.; Lee, B.; Lee, G.; Floresca, C.; Cha, P.-R.; Ahn, J.; Wallace, R. M.; Chabal, Y. J.; Kim, M. J.; *et al.* Atomic Layer Deposition of Dielectrics on Graphene Using Reversibly Physisorbed Ozone. *ACS Nano* **2012**, *6*, 2722–2730.
49. Wang, L.; Travis, J. J.; Cavanagh, A. S.; Liu, X.; Koenig, S. P.; Huang, P. Y.; George, S. M.; Bunch, J. S. Ultrathin Oxide Films by Atomic Layer Deposition on Graphene. *Nano Lett.* **2012**, *12*, 3706–3710.
50. Sangwan, V. K.; Jariwala, D.; Filippone, S. A.; Karmel, H. J.; Johns, J. E.; Alaboson, J. M. P.; Marks, T. J.; Lauhon, L. J.; Hersam, M. C. Quantitatively Enhanced Reliability and Uniformity of High-κ Dielectrics on Graphene Enabled by Self-Assembled Seeding Layers. *Nano Lett.* **2013**, *13*, 1162–1167.
51. Hall, R. A.; Yoon, B.; Cavanagh, A.; George, S. M. Molecular Layer Deposition of Hybrid Organic-Inorganic Films Using Trimethylaluminum and Multifunctional Organic Precursors, to be submitted for publication, **2013**.
52. Hall, R. A. Metalcone Chemistry: In *Pursuit of Improved Mechanical Properties in Thin Film Deposition*. Ph.D. Dissertation [Online], University of Colorado, Boulder, CO, 2013. http://search.proquest.com/docview/1367594861 (accessed July 16, 2013).

53. Hall, R. A.; George, S. M. Molecular Layer Deposition of the Hybrid Inorganic-Organic Film Zinc (II) Glycerolate, to be submitted for publication, **2013**.
54. Abdulagatov, A. I.; Hall, R. A.; Sutherland, J. L.; Lee, B. H.; Cavanagh, A. S.; George, S. M. Molecular Layer Deposition of Titanicone Films Using $TiCl_4$ and Ethylene Glycol or Glycerol: Growth and Properties. *Chem. Mater.* **2012**, *24*, 2854–2863.
55. Miller, D. C.; Foster, R. R.; Jen, S.-H.; Bertrand, J. A.; Seghete, D.; Yoon, B.; Lee, Y.-C.; George, S. M.; Dunn, M. L. Thermo-mechanical Properties of Aluminum Alkoxide (Alucone) Films Created Using Molecular Layer Deposition. *Acta Mater.* **2009**, *57*, 5083–5092.
56. Tripp, M. K.; Stampfer, C.; Miller, D. C.; Helbling, T.; Herrmann, C. F.; Hierold, C.; Gall, K.; George, S. M.; Bright, V. M. The Mechanical Properties of Atomic Layer Deposited Alumina for Use in Micro- and Nano-Electromechanical Systems. *Sens. Actuators, A* **2006**, *130*−*131*, 419–429.
57. Jen, S.-H.; Bertrand, J. A.; George, S. M. Critical Tensile and Compressive Strains for Cracking of Al_2O_3 Films Grown by Atomic Layer Deposition. *J. Appl. Phys.* **2011**, *109*, 084305.
58. Bull, S. J. Mechanical Response of Atomic Layer Deposition Alumina Coatings on Stiff and Compliant Substrates. *J. Vac. Sci. Technol., A* **2012**, *30*, 01A160.
59. Lee, B. H.; Anderson, V. R.; George, S. M. Molecular Layer Deposition of Zircone and ZrO_2/Zircone Alloy Films: Growth and Properties. *Chem. Vap. Deposition* **2013**, *19*, 204–212.
60. Lee, B. H.; Yoon, B.; Abdulagatov, A. I.; Hall, R. A.; George, S. M. Growth and Properties of Hybrid Organic-Inorganic Metalcone Films Using Molecular Layer Deposition Techniques. *Adv. Funct. Mater.* **2013**, *23*, 532–546.
61. Zhang, L.; Prosser, J. H.; Feng, G.; Lee, D. Mechanical Properties of Atomic Layer Deposition-Reinforced Nanoparticle Thin Films. *Nanoscale* **2012**, *4*, 6543–6552.
62. Riley, L. A.; Cavanagh, A. S.; George, S. M.; Lee, S.-H.; Dillon, A. C. Improved Mechanical Integrity of ALD-Coated Composite Electrodes for Li-Ion Batteries. *Electrochem. Solid-State Lett.* **2011**, *14*, A29–A31.
63. Dafinione, M. I.; Feng, G.; Brugarolas, T.; Tettey, K. E.; Lee, D. Mechanical Reinforcement of Nanoparticle Thin Films Using Atomic Layer Deposition. *ACS Nano* **2011**, *5*, 5078–5087.
64. Landi, B. J. Rochester Institute of Technology, Rochester, NY. Personal communication, **2012**.
65. Landi, B. J.; Cress, C. D.; Evans, C. M.; Raffaelle, R. P. Thermal Oxidation Profiling of Single Walled Carbon Nanotubes. *Chem. Mater.* **2005**, *17*, 6819–6834.
66. Saito, R.; Dresselhaus, G.; Dresselhaus, M. S. *Physical Properties of Carbon Nanotubes*; Imperial College Press: London, 1998; p 210.
67. Min, J.; Cai, J. Y.; Sridhar, M.; Easton, C. D.; Gengenbach, T. R.; McDonnell, J.; Humphries, W.; Lucas, S. High Performance Carbon Nanotube Spun Yarns from a Crosslinked Network. *Carbon* **2013**, *52*, 520–527.
68. Deng, F.; Ogasawara, T.; Takeda, N. Evaluating the Orientation and Dispersion of Carbon Nanotubes Inside Nanocomposites by a Focused-Ion-Beam Technique. *Mater. Lett.* **2007**, *61*, 5095–5097.
69. Ke, X.; Bals, S.; Negreira, A. R.; Hantschel, T.; Bender, H.; Tendeloo, G. V. TEM Sample Preparation by FIB for Carbon Nanotube Interconnects. *Ultramicroscopy* **2004**, *109*, 1353–1359.
70. Raghuveer, M. S.; Ganesan, P. G.; D'Arcy-Gall, J.; Ramanath, G.; Marshall, M.; Petrov, I. Nanomachining Carbon Nanotubes with Ion Beams. *Appl. Phys. Lett.* **2004**, *84*, 4484–4486.
71. Krenchel, H. Fibre Reinforcement; Akademisk Forlag: Copenhagen, 1964. As quoted in Callister, W. D., Jr. *Materials Science and Engineering: An Introduction*, 7th ed.; Wiley: New York, 2007; p 594.
72. Elam, J. W.; Groner, M. D.; George, S. M. Viscous Flow Reactor with Quartz Crystal Microbalance for Thin Film Growth by Atomic Layer Deposition. *Rev. Sci. Instrum.* **2002**, *73*, 2981–2987.